Solid-state NMR and EPR Spectroscopy of Mn2+-Substituted ATP-Fueled Protein Engines

Author(s):
Wiegand, Thomas; Lacabanne, Denis; Keller, Katharina; Cadalbert, Riccardo; Lecoq, Lauriane; Yulikov, Maxim; Terradot, Laurent; Jeschke, Gunnar; Meier, Beat H.; Böckmann, Anja

Publication date:
2017-03-13

Permanent link:
https://doi.org/10.3929/ethz-b-000128825

Originally published in:
Angewandte Chemie. International Edition 56(12), https://doi.org/10.1002/anie.201610551

Funding acknowledgement:
159707 - NMR studies in the Solid State (SNF)
146757 - NMR studies in the Solid State (SNF)
169057 - Generation of spin-label based restraints on biomolecular structure and their use in hybrid structure modelling (SNF)

Solid-state NMR and EPR of Mn^{2+} substituted ATP-fueled protein engines

Thomas Wiegand,[a]# Denis Lacabanne,[b]# Katharina Keller,[a]# Riccardo Cadalbert,[a] Lauriane Lecoq,[b] Maxim Yulikov,[a] Laurent Terradot*[b], Gunnar Jeschke,*[a] Beat H. Meier*[a] and Anja Böckmann*[b]

[a] Dr. Thomas Wiegand, Katharina Keller, Riccardo Cadalbert, Dr. Maxim Yulikov, Prof. Gunnar Jeschke, Prof. Beat H. Meier
Physical Chemistry
ETH Zurich
8093 Zurich, Switzerland
E-mail: beme@ethz.ch, gunnar.jeschke@phys.chem.ethz.ch

[b] Denis Lacabanne, Dr. Lauriane Lecoq, Dr. Laurent Terradot, Dr. Anja Böckmann,
Molecular Microbiology and Structural Biochemistry, Labex Ecofect, UMR 5086 CNRS/Université de Lyon
69367 Lyon, France

# equal contributions

Abstract: Paramagnetic metal ions provide structural information both in EPR and solid-state NMR experiments, offering a profitable synergetic approach to study bio-macromolecules. We demonstrate the spectral consequences of Mg^{2+}/ Mn^{2+} substitution and resulting information contents for two different ATP:Mg^{2+}-fueled protein engines, a DnaB helicase from *Helicobacter Pylori* active in the bacterial replisome, and the ABC transporter BmrA, a bacterial efflux pump. We show that, while EPR spectra report on metal binding and inform on the geometry of the metal centers in the proteins, paramagnetic relaxation enhancements identified in the NMR spectra can be used to localize residues at the binding site. Protein engines are ubiquitous and the methods described here should be applicable in a broad context.

Nucleotide binding domains (NBDs) are multipurpose engines which convert the chemical energy released on nucleoside triphosphate hydrolysis into mechanical movement or switching. They are found in a set of proteins for which conformational change and molecular motion is needed for function,[1,2] with adenosine triphosphate (ATP) being a common fuel for these engines. We here inquire what information on ATP binding to NBDs can be obtained by an approach that combines data from paramagnetic solid-state NMR[3-6] and from EPR spectroscopy when Mg^{2+} as a cofactor of ATP hydrolysis is replaced by Mn^{2+}. For this, we focus on a helicase (*Hp*DnaB)[7] and an ABC transporter (BmrA)[8] as two proteins whose function relies on NBDs,[9] but with nucleotide-binding dissociation constants (Kd) differing by roughly two orders of magnitude.[10-12] For ATP hydrolysis, which provides the energy source for the engine, the NBDs require a divalent metal ion, typically Mg^{2+}, as cofactor. Both proteins show multiple ATP binding sites: 12 for *Hp*DnaB, and two for BmrA. Each domain contains Walker A and B motifs, with an aspartate that coordinates Mg^{2+}. While in the helicase the NBDs maintain contact throughout the functional cycle, they are spatially separated in the ABC transporter BmrA in the open conformation and assemble to bind and hydrolyze ATP:Mg^{2+}. In order to mimic nucleotide-bound states, poorly hydrolysable analogues can be used, such as adenylyl-imidodiphosphate (AMP-PNP), which binds with high affinity to *Hp*DnaB.[7,13] The dissociation constants of BmrA-nucleotide complexes in the absence of substrate[12] is larger than the ones of DnaB[10,11] and large amounts of AMP-PNP/metal would be needed for the preparation of an NMR sample showing high occupancy of the binding sites, and we instead used ATP:VO_4^{3-}:Mg^{2+}. After ATP hydrolysis in the presence of vanadate, the NBDs are expected to remain blocked in an ADP:VO_4^{3-}:Mg^{2+} bound state, with the VO_4^{3-} ion mimicking the γ-phosphate of ATP.[14]

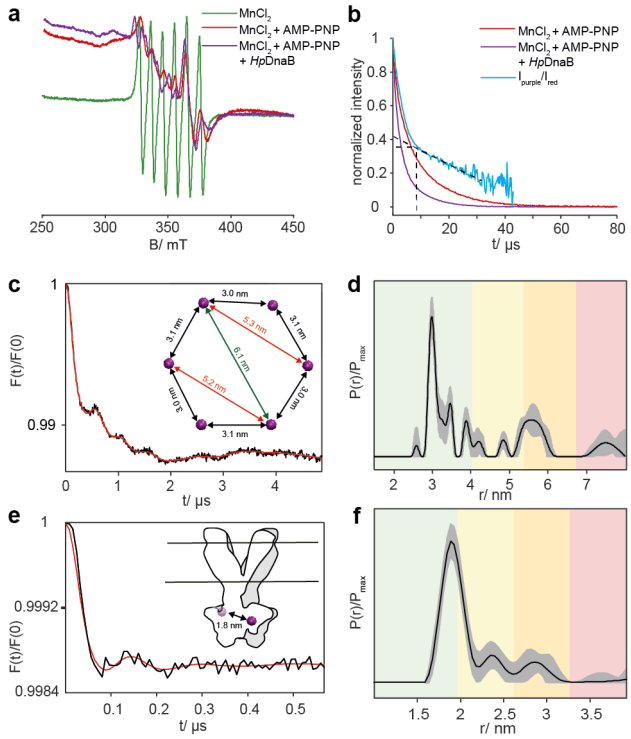

Figure 1. (a) Mn^{2+} X-band CW spectra at room temperature of a $MnCl_2$ (green), a AMP-PNP:Mn^{2+} (red) and a *Hp*DnaB:AMP-PNP:Mn^{2+} solution with *Hp*DnaB:Mn^{2+} 12:1 (purple). For CW spectra of the 1:1 complex see the Supplemental Materials Section.) (b) Mn^{2+} Hahn echo decay curves of AMP-PNP:Mn^{2+} and *Hp*DnaB:AMP-PNP:Mn^{2+} (*Hp*DnaB:Mn^{2+} 1:1) at 20 K and division of the normalized decaying functions of AMP-PNP:Mn^{2+} and *Hp*DnaB:AMP-PNP:Mn^{2+} (blue). The faster decay indicates binding of Mn^{2+} to the protein. About 60 % of the nucleotide binding sites of the helicase are occupied by AMP-PNP:Mn^{2+}. (c) Mn^{2+}-Mn^{2+} ultra wideband DEER form factor (black) and simulated form factor corresponding to the distance distribution (red) and (d) distance distribution at a temperature of 10 K for *Hp*DnaB (green, shape of distance distribution is reliable; yellow, mean distance and width are reliable; orange, mean distance is reliable; red, long-range distance contributions may be detectable, but cannot be quantified). Grey indicates uncertainty revealed by the validation of the background range and by introduction of artificial noise (see Material and Methods Section in SI). The nearest-neighbor Mn^{2+}-Mn^{2+} distance of 3 nm expected from the homology model (see inset in c) can be detected with high significance and there is an indication for distances between 5 and 6 nm. The DEER experiments were recorded on a deuterated sample with a 1:1.5 protein:Mn^{2+} ratio. (e) BmrA:ADP:Mn^{2+}:VO_4^{3-} Mn^{2+}-Mn^{2+} ultra wideband DEER form factor (black) and simulated form factor corresponding to the distance distribution (red) and (f) distance distribution at a temperature of 10 K for Mn^{2+} in BmrA:ADP:Mn^{2+}:VO_4^{3-}. The maximum at 1.9 nm agrees well with the Mn^{2+}-Mn^{2+} distance predicted from a homology model (see inset in e)). Colors as in (d).

The characterization of the interaction between ATP and the NBDs is essential for understanding the functioning of such ATP-fueled proteins. By substituting the diamagnetic Mg^{2+} by paramagnetic Mn^{2+}, the binding sites become EPR observable[15,16] and a distance-dependent paramagnetic relaxation enhancement (PRE) is induced for the NMR resonances.[17-21] This provides contrast between the binding site and the part of the system remote from it. Due to similar coordination behavior, charge and ion radius of Mg^{2+} and Mn^{2+} ions, most often function is retained ([22] and Figure S1).

We added Mn^{2+} and ATP analogues to the two proteins in order to demonstrate the effects of nucleotide:Mn^{2+} binding on NMR and EPR spectra. This allows to determine the occupation of nucleotide binding sites, to extract Mn^{2+}-Mn^{2+} distances,[23] to probe the geometry of the multimeric assemblies, as well as to identify the residues in the neighborhood of Mn^{2+}. The radius of view is on the order of 15 Å for residue identification and on the order of 35-65 Å for assembly geometry

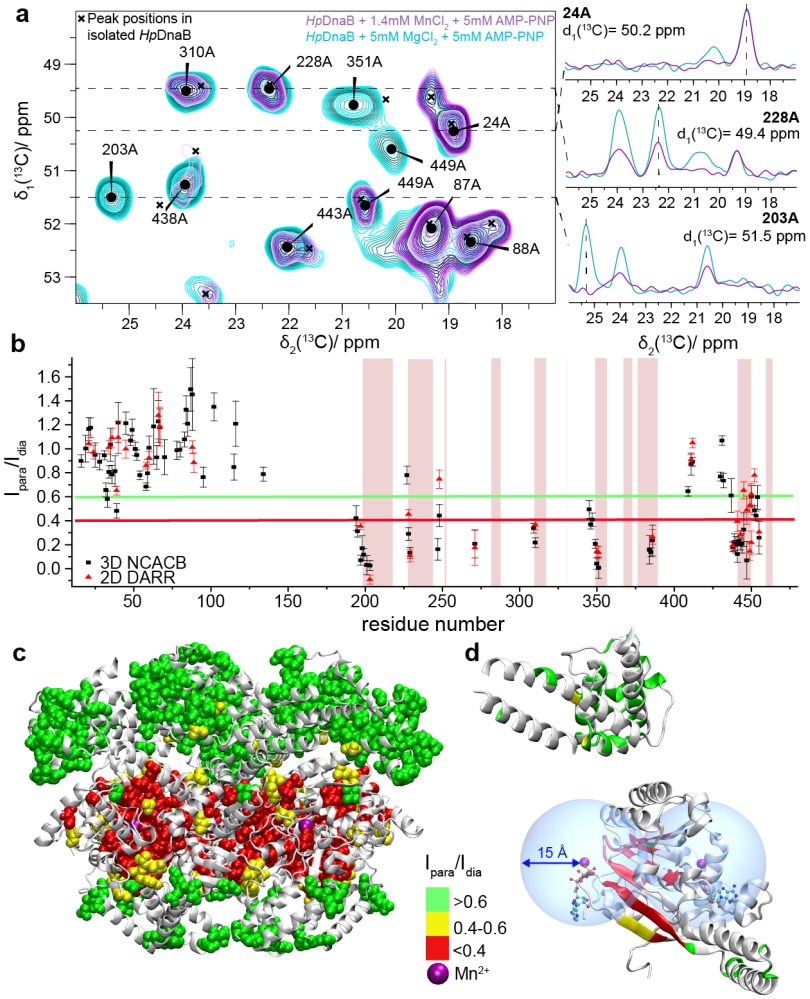

Figure 2. 2D ^{13}C-^{13}C DARR spectra showing the Ala region of the *Hp*DnaB:AMP-PNP:Mg^{2+} (cyan) and of the *Hp*DnaB:AMP-PNP:Mn^{2+} (purple) complexes. 1D traces along F2 are shown for (i) unaffected resonances (24A), (ii) attenuated resonances (228A) and (iii) disappearing resonances (203A). (b) PRE effects (black squares: determined from 3D NCACB spectra, red triangles: determined from 2D DARR spectra). Residues with effective distances < 15 Å (distance between Cα and the two nearest metals) (see Figure S8) are highlighted in red. The red and green horizontal lines indicate I_{para}/I_{dia} values of 0.4 and 0.6 which we consider as bounds for residues experiencing strong (<0,4) and no PRE effects (>0.6). (c) *Hp*DnaB hexamer with PRE effects determined from 3D NCACB spectra plotted as vdW balls. (d) Zoom into one *Hp*DnaB monomer with PRE effects plotted on the structure. Spheres with R = 15 Å around the Mn^{2+} ions from two adjacent monomers are shown in blue.

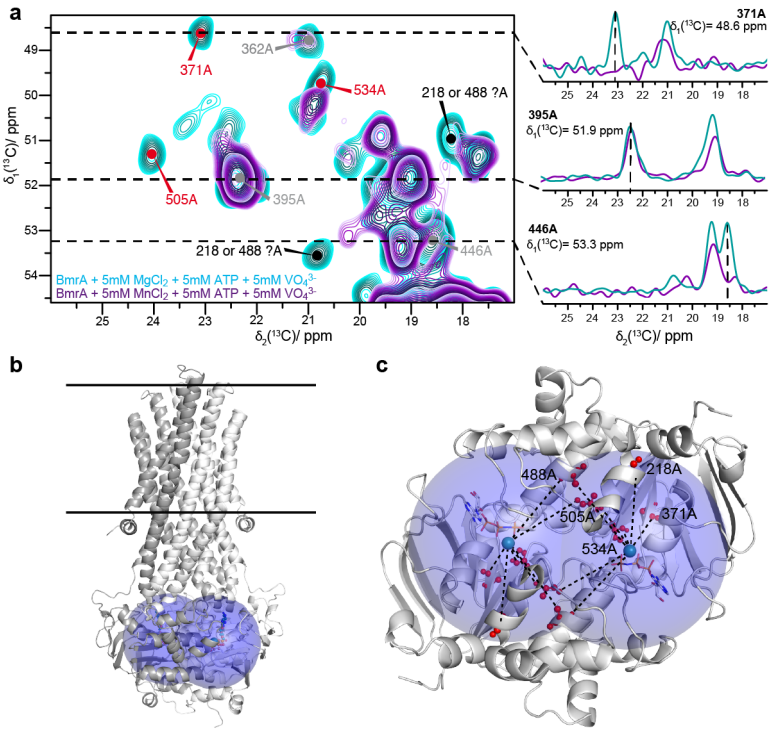

Figure 3. a) Alanine region from 2D ^{13}C-^{13}C DARR spectra of the BmrA:ADP:Mg^{2+}:VO_4^{3-} (cyan) and of the BmrA:ADP:Mn^{2+}:VO_4^{3-} (purple) complexes. Residues are labeled in red/black for assigned/unassigned Ala within 15 Å of the Mn^{2+}, and in grey for Ala outside this limit. Representative 1D traces along F2 are shown as insets with examples for disappearing, unaffected and attenuated resonances respectively. b) BmrA model obtained by homology from the ABC transporter SAV1866 x-ray structure[24] (2HYD) embedded in lipid bilayers represented by horizontal lines. The spheres shown in blue are centered at the Mg^{2+} and show a radius of 15 Å. c) Plot of the nucleotide binding domain and all Ala residues (red) located within 15 Å radius from the metal (cyan).

EPR allows to follow the binding of Mn^{2+} to the NBD. Figure 1a shows the room temperature X-band Mn^{2+} CW spectra of the *Hp*DnaB:AMP-PNP:Mn^{2+} complex in solution, as well as of $MnCl_2$ and AMP-PNP:Mn^{2+} solutions as reference. The spectrum of the $MnCl_2$ solution consists of a resolved sextet for the $|-1/2,M_I\rangle \leftrightarrow |+1/2,M_I\rangle$ transitions due to the electron-^{55}Mn hyperfine splitting of about 8 mT, as expected for the fast tumbling high-spin Mn^{2+} hexaaquo complex (S=5/2 and *I*=5/2). Addition of AMP-PNP leads to formation of a larger complex with longer rotational correlation time and lower symmetry and thus to an anisotropic broadening of the resonance and to additional spectral features due to the zero-field splitting. The observed spectrum indicates quantitative formation of the nucleotide-metal complex for the case of a 1:12 Mn^{2+}:*Hp*DnaB monomer ratio. The binding of the nucleotide-metal complex to the *Hp*DnaB helicase causes a further prolongation of the rotational correlation time and thus a further change of the EPR line shape as well as changes in the zero-field splitting parameters, which are expected from the changes in the ligand field (see Figure S2 for EDEPR spectra at 10 K showing the influence of differences in the zero-field splitting on the EPR lineshape). Protein binding can even better be apprehended by the Mn^{2+} transverse relaxation curves shown in Figure 1b (see also Figure S3 for results on a deuterated *Hp*DnaB). For the protein complex we observe bimodal Mn^{2+} relaxation behavior, indicating that AMP-PMP:Mn^{2+} complexes bound to the NBDs relax significantly faster than the isolated AMP-PMP:Mn^{2+} in buffer solution. This is probably due to the close vicinity of up to five other Mn^{2+} ions, as well as fluctuating hyperfine fields caused by proton spin-diffusion in the helicase that strongly exceed the fluctuating fields in the deuterated buffer matrix of the unbound complex. The binding efficiency can be determined in good approximation[25,26] by dividing the normalized *Hp*DnaB:AMP-PNP:Mn^{2+} and AMP-PNP:Mn^{2+} transverse relaxation traces (see SI). The slowly decaying component crosses the vertical axis at a value of 0.4, indicating that about 60 % of AMP-PMP:Mn^{2+} complexes are bound to NBDs for the case of a 1:1 Mn^{2+}/*Hp*DnaB monomer ratio (this leads to a K_d value in the order of 10^{-5} M in agreement with published values for similar proteins).[10,11] We thus used for NMR experiments a five-fold excess of Mn^{2+} and an 18-fold excess of AMP-PNP to occupy all binding sites. Typical ATP concentrations in bacteria range from about 1 to 10 mM[27,28] and may exceed NBD concentration by an even larger ratio. The distribution of the Mn^{2+}-Mn^{2+} distances was determined by Double Electron Electron Resonance (DEER) with broadband chirp pump pulses (see Material and Methods Section in SI) in order to obtain a measurable dipolar modulation depth in spite of the large width of Mn^{2+} EPR spectrum.[29-32] Figure 1c shows the DEER form factor trace obtained as a sum of two measurements on a *Hp*DnaB:AMP- PNP:Mn^{2+} sample (see Material and Methods Section in SI and Figure S4 for a detailed description), and Figure 1d the resulting distance distribution obtained by Tikhonov regularization analysis.[33] Distances of 3 nm and, with lower significance, of 5-6 nm are found, showing that the (double-) hexameric assembly in *Hp*DnaB (Figure 1f) is conserved, with slight deviations from the homology model based on the *Aa*DnaB:ADP:Mg^{2+} complex[34] being expected. Peaks in the range between 3.4 and 4 nm are less significant and may be related to flexibility or to unspecifically bound Mn^{2+}. Due to the low inversion efficiency of even the ultra-wideband pump pulses, multispin contributions in the multimeric assembly[35,36] are not expected in our case.

The 2D DARR ^{13}C-^{13}C NMR correlation spectra[37] of the diamagnetic *Hp*DnaB:AMP-PNP:Mg^{2+} and paramagnetic *Hp*DnaB:AMP-PNP:Mn^{2+} complexes are given in Figure S5, and zoom to the alanine region in Figure 2a. (Thr/Ile/Val regions in Figures S6 and S7). Assignments are taken from ref.[13,38] Three types of resonances can be distinguished in the 2D spectra: (i) residues unaffected by Mn^{2+} (e.g. 24A), (ii) residues attenuated by Mn^{2+} PRE (e.g. 228A, 310A) and (iii) resonances disappearing at the given signal-to-noise ratio because of strong PRE (e.g. 203A, 351A). Figure 2a further reveals that all nucleotide binding sites are occupied by AMP-PNP:Mn^{2+}, since resonances do not split, but shift completely. The peak intensity in the 2D spectra is influenced by the faster T_1, $T_{1\rho}$ and T_2 relaxation, resulting in a reduced signal intensity due to losses during the polarization-transfer periods and T_2 broadening, respectively.[21] PRE scales with r^6, r being the distance between the metal center and a protein nucleus. The radius of the sphere around Mn^{2+} with significant PRE depends on the T_1 relaxation time of unpaired electrons of Mn^{2+}, which cannot easily be measured at a temperature of 278 K. According to a homology model of *Hp*DnaB, based on *Aa*DnaB, the radius of view can be estimated to be 15 Å. Further site-specific PRE data were obtained from 3D NCACB spectra (Figure S9) and are summarized in Figure 2b. The N-terminal domain is hardly affected by Mg^{2+}/Mn^{2+} substitution, whereas parts of the NBD containing C-terminal domain (CTD) experience strong PREs (I_{para}/I_{dia}<0.4). Stretches of residues with Cα atoms closer than 15 Å to the Mn^{2+} are marked as vertical red bars and show strong PREs. The agreement is not perfect, probably due to the limitations of the homology model. Figure 2c shows a side view on one *Hp*DnaB hexamer model with the PRE effects plotted on the structure. Significant PRE's indeed only appear in the CTD in vicinity of the paramagnetic centers (in contrast to chemical-shift perturbations (CSPs), which can be a consequence of both proximal and allosteric changes[39]). An alternative view is provided in Figure 2d where spheres with a radius of 15 Å are plotted around the metal centers showing that resonances within this sphere are strongly affected by PRE effects upon Mn^{2+} binding. The PRE determined here correlate with the CSPs upon AMP-PNP:Mg^{2+} binding that were determined earlier (see Figure S10).[13]

In order to compare the effects of Mn^{2+} for a protein which shows lower nucleotide binding constants, we investigated the ABC transporter BmrA, for which a larger excess of Mn^{2+} compared to a BmrA monomer is used to obtain quantitative binding (300-fold excess compared to 5-fold in *Hp*DnaB). The alanine region of the 2D DARR ^{13}C-^{13}C NMR correlation spectra of BmrA, recorded on a reverse labeled ^{12}C-^{14}N-[LVIKHP]-^{13}C-^{15}N sample of BmrA:ADP:Mn^{2+}:VO_4^{3-}, is shown in Figure 3a in purple. The full aliphatic region, as well as the Ser and Thr regions, are shown in Figures S11 and S12 respectively. When comparing this spectrum to the one of diamagnetic BmrA:ADP:Mg^{2+}:VO_4^{3-}, one can also observe - as in the case of *Hp*DnaB discussed above - non-attenuated, attenuated and disappearing resonances in the presence of the paramagnetic ion. From a set of assigned Ala residues (Figure S13) we find that the peaks of 371A, 505A and 534A show strong PRE in accordance with a homology model (based on Sav1866[24]) where these residues are indeed located within a sphere of 15 Å from the metal center (Figure S14). Two more alanine residues within this radius, 488A and 218A, can likely be assigned to the two additional disappearing signals labeled in black in Figure 3a. Two additional assigned Ala residues outside the 15 Å sphere show also attenuation by PREs. We note that 446A has four nearby negatively charged residues as neighbors, 442D, 445D, 447E and 449E. A closer look at the C' side chain region displaying mainly Glu Cδ and Asp Cγ resonances reveals that most corresponding signals are significantly attenuated. As Asp and Glu are good binders of Mn^{2+},[40] this is likely due to the surplus Mn^{2+} with the negatively charged side chains of these residues (see also Figure S15a). In line with this, the Glu Cγ/Cδ cross signal is attenuated by about 80 % (Figure S15b). The attenuation of the Cβ/Cγ cross signals is already smaller (<45 %), indicating that the effect is local and smaller than the one exerted by Mn^{2+} located in the nucleotide binding site, probably due to fast chemical exchange of the surface-bound Mn^{2+} with Mn^{2+} in solution. The residues located in the trans-membrane helices are not influenced by PRE, as can be seen at the signals of the α-helical Ala residues, which are the least affected peaks in the spectra, and have been used to calibrate the two spectra with respect to each other (Figure S15c). Mn^{2+}-Mn^{2+} distance distributions in BmrA:ADP:Mn^{2+}:VO_4^{3-} could be determined by DEER experiments despite the low modulation depths due to the larger amount of free Mn^{2+} (see Figures 1 e,f and for details see Supplemental Materials Sections, notably Figures S16 to S19). The distance distribution has a maximum at about 1.9 nm, which is in agreement with the Mn^{2+}-Mn^{2+} distances in the homology model of BmrA:ADP:Mn^{2+}:VO_4^{3-} representing the closed form (1.8 nm).

In summary, we have demonstrated on two examples that NBD engines in proteins can be investigated by the exchange of diamagnetic Mg^{2+} with paramagnetic Mn^{2+}. No tagging is necessary, and no distribution of metal positions, like in flexible tags, exists. Pulsed EPR methods, in particular ultra-wideband DEER, allow for the evaluation of distances between paramagnetic centers in the multimers. The measurement of PREs in solid-state NMR identifies the residues close to the binding site unambiguously, in contrast to CSPs that cannot distinguish direct and allosteric effects. Additional unspecific binding to solvent-exposed sidechains was observed in BmrA due to the higher Mn^{2+} concentrations. They act, however, in a smaller radius of a few Å and do not hinder the characterization of the binding site. The spectroscopic approaches described here should be generally applicable to the study of the many proteins possessing ATP-fueled engines, and a combination of approaches should allow deeper insights in the mechanisms powering these machines, and also the remote conformational changes driven by the engines.

Experimental Section

See Supporting Information

Acknowledgements

We would like to thank Cédric Orelle and Jean-Michel Jault (MMSB Lyon) for guiding us for activity testing of BmrA in presence of Mn^{2+}; Simon Widler for support with the sample preparation; as well as Andrin Doll and Frauke Breitgoff for introduction to the AWG setup. This work was supported by the Swiss National Science Foundation (Grant 200020_159707, 200020_146757 and 200020_157034), the French ANR (ANR-14-CE09-0024B) and the ETH Career SEED-69 16-1.

Keywords: NMR spectroscopy • EPR spectroscopy • Manganese • Membrane proteins • DNA replication

[1] P. I. Hanson, S. W. Whiteheart, *Nat Rev Mol Cell Biol* **2005**, *6*, 519–529.
[2] D. C. Rees, E. Johnson, O. Lewinson, *Nat Rev Mol Cell Biol* **2009**, *10*, 218–227.
[3] C. P. Jaroniec, *J. Magn. Reson.* **2015**, *253*, 50–59.
[4] S. J. Ullrich, S. Hölper, C. Glaubitz, *J. Biomol. NMR* **2014**, *58*, 27–35.
[5] I. Bertini, L. Emsley, M. Lelli, C. Luchinat, J. Mao, G. Pintacuda, *J. Am. Chem. Soc.* **2010**, *132*, 5558–5559.
[6] G. Pintacuda, N. Giraud, R. Pierattelli, A. Böckmann, I. Bertini, L. Emsley, *Angew Chem Int Ed Engl* **2007**, *46*, 1079–1082.
[7] A. Bazin, M. V. Cherrier, I. Gutsche, J. Timmins, L. Terradot, *Nucleic Acids Res.* **2015**, gkv792–13.
[8] E. Steinfels, C. Orelle, J.-R. Fantino, O. Dalmas, J.-L. Rigaud, F. Denizot, A. Di Pietro, J.-M. Jault, *J. Biol. Chem.* **2004**, *43*, 7491–7502.
[9] C. Geourjon, C. Orelle, E. Steinfels, C. Blanchet, G. Deléage, A. Di Pietro, J. M. Jault, *Trends in Biochemical Sciences* **2001**, *26*, 539–544.
[10] W. Bujalowski, M. M. Klonowska, *J. Biol. Chem.* **1993**, *32*, 5888–5900.
[11] M. J. Jezewska, U. S. Kim, W. Bujalowski, *Biophysical Journal* **1996**, *71*, 2075–2086.
[12] A. Siarheyeva, R. Liu, F. J. Sharom, *Journal of Biological Chemistry* **2010**, *285*, 7575–7586.
[13] T. Wiegand, R. Cadalbert, C. Gardiennet, J. Timmins, L. Terradot, A. Böckmann, B. H. Meier, *Angew. Chem. Int. Ed.* **2016**, DOI 10.1002/anie.201607295.
[14] C. Orelle, F. Gubellini, A. Durand, S. Marco, D. Lévy, P. Gros, A. [1] P. I. Hanson, S. W. Whiteheart, *Nat Rev Mol Cell Biol* **2005**, *6*, 519–529.
[2] D. C. Rees, E. Johnson, O. Lewinson, *Nat Rev Mol Cell Biol* **2009**, *10*, 218–227.
[3] C. P. Jaroniec, *J. Magn. Reson.* **2015**, *253*, 50–59.
[4] S. J. Ullrich, S. Hölper, C. Glaubitz, *J. Biomol. NMR* **2014**, *58*, 27–35.
[5] I. Bertini, L. Emsley, M. Lelli, C. Luchinat, J. Mao, G. Pintacuda, *J. Am. Chem. Soc.* **2010**, *132*, 5558–5559.
[6] G. Pintacuda, N. Giraud, R. Pierattelli, A. Böckmann, I. Bertini, L. Emsley, *Angew Chem Int Ed Engl* **2007**, *46*, 1079–1082.
[7] A. Bazin, M. V. Cherrier, I. Gutsche, J. Timmins, L. Terradot, *Nucleic Acids Res.* **2015**, gkv792–13.
[8] E. Steinfels, C. Orelle, J.-R. Fantino, O. Dalmas, J.-L. Rigaud, F. Denizot, A. Di Pietro, J.-M. Jault, *J. Biol. Chem.* **2004**, *43*, 7491–7502.
[9] C. Geourjon, C. Orelle, E. Steinfels, C. Blanchet, G. Deléage, A. Di Pietro, J. M. Jault, *Trends in Biochemical Sciences* **2001**, *26*, 539–544.
[10] W. Bujalowski, M. M. Klonowska, *J. Biol. Chem.* **1993**, *32*, 5888–5900.
[11] M. J. Jezewska, U. S. Kim, W. Bujalowski, *Biophysical Journal* **1996**, *71*, 2075–2086.
[12] A. Siarheyeva, R. Liu, F. J. Sharom, *Journal of Biological Chemistry* **2010**, *285*, 7575–7586.
[13] T. Wiegand, R. Cadalbert, C. Gardiennet, J. Timmins, L. Terradot, A. Böckmann, B. H. Meier, *Angew. Chem. Int. Ed.* **2016**, DOI 10.1002/anie.201607295.
[14] C. Orelle, F. Gubellini, A. Durand, S. Marco, D. Lévy, P. Gros, A. Di Pietro, J.-M. Jault, *J. Biol. Chem.* **2008**, *47*, 2404–2412.
[15] H. Witt, A. Wittershagen, E. Bill, B. O. Kolbesen, B. Ludwig, *FEBS Letters* **1997**, *409*, 128–130.
[16] M. Bennati, M. M. Hertel, J. Fritscher, T. F. Prisner, N. Weiden, R. Hofweber, M. Spörner, G. Horn, H. R. Kalbitzer, *J. Biol. Chem.* **2006**, *45*, 42–50.
[17] E. Bonneau, P. Legault, *J. Biol. Chem.* **2014**, *53*, 579–590.
[18] I. Bertini, C. Luchinat, G. Parigi, R. Pierattelli, *Chembiochem* **2005**, *6*, 1536–1549.
[19] H. Kaur, A. Lakatos, R. Spadaccini, R. Vogel, C. Hoffmann, J. Becker-Baldus, O. Ouari, P. Tordo, H. Mchaourab, C. Glaubitz, *Biol. Chem.* **2015**, *0*, DOI 10.1515/hsz-2015-0119.
[20] G. Otting, *Annu. Rev. Biophys.* **2010**, *39*, 387–405.
[21] H. Tamaki, A. Egawa, K. Kido, T. Kameda, M. Kamiya, T. Kikukawa, T. Aizawa, T. Fujiwara, M. Demura, *J. Biomol. NMR* **2016**, *64*, 87–101.
[22] R. K. Soni, P. Mehra, N. R. Choudhury, G. Mukhopadhyay, S. K. Dhar, *Nucleic Acids Res.* **2003**, *31*, 6828–6840.
[23] H. Y. V. Ching, F. C. Mascali, H. C. Bertrand, E. M. Bruch, P. Demay-Drouhard, R. M. Rasia, C. Policar, L. C. Tabares, S. Un, *J. Phys. Chem. Lett.* **2016**, *7*, 1072–1076.
[24] R. J. P. Dawson, K. P. Locher, *FEBS Letters* **2007**, *581*, 935–938.
[25] P. Lueders, S. Razzaghi, H. Jäger, R. Tschaggelar, M. A. Hemminga, M. Yulikov, G. Jeschke, *Mol Phys* **2013**, *111*, 2824–2833.
[26] S. Razzaghi, E. K. Brooks, E. Bordignon, W. L. Hubbell, M. Yulikov, G. Jeschke, *Chembiochem* **2013**, *14*, 1883–1890.
[27] H. Yaginuma, S. Kawai, K. V. Tabata, K. Tomiyama, A. Kakizuka, T. Komatsuzaki, H. Noji, H. Imamura, *Sci. Rep.* **2014**, *4*, 6522.
[28] B. D. Bennett, E. H. Kimball, M. Gao, R. Osterhout, S. J. Van Dien, J. D. Rabinowitz, *Nat. Chem. Biol.* **2009**, *5*, 593–599.
[29] M. Pannier, S. Veit, A. Godt, G. Jeschke, H. W. Spiess, *J. Magn. Reson.* **2011**, *213*, 316–325.
[30] A. Doll, M. Qi, N. Wili, S. Pribitzer, A. Godt, G. Jeschke, *J. Magn. Reson.* **2015**, *259*, 153–162.
[31] D. Banerjee, H. Yagi, T. Huber, G. Otting, D. Goldfarb, *J. Phys. Chem. Lett.* **2012**, *3*, 157–160.
[32] H. Y. Vincent Ching, P. Demay-Drouhard, H. C. Bertrand, C. Policar, L. C. Tabares, S. Un, *Phys. Chem. Chem. Phys.* **2015**, *17*, 23368–23377.
[33] G. Jeschke, V. Chechik, P. Ionita, A. Godt, H. Zimmermann, J. Banham, C. R. Timmel, D. Hilger, H. Jung, *Appl Magn Reson* **2006**, *30*, 473–498.
[34] M. S. Strycharska, E. Arias-Palomo, A. Y. Lyubimov, J. P. Erzberger, V. L. O'Shea, C. J. Bustamante, J. M. Berger, *Molecular Cell* **2013**, *52*, 844–854.
[35] C. Pliotas, R. Ward, E. Branigan, A. Rasmussen, G. Hagelueken, H. Huang, S. S. Black, I. R. Booth, O. Schiemann, J. H. Naismith, *PNAS* **2012**, *109*, E2675–82.
[36] S. Valera, K. Ackermann, C. Pliotas, H. Huang, J. H. Naismith, B. E. Bode, *Chem. Eur. J.* **2016**, *22*, 4700–4703.
[37] K. Takegoshi, S. Nakamura, T. Terao, *J Chem Phys* **2003**, *118*, 2325.
[38] T. Wiegand, C. Gardiennet, F. Ravotti, A. Bazin, B. Kunert, D. Lacabanne, R. Cadalbert, P. Güntert, L. Terradot, A. Böckmann, et al., *Biomol NMR Assign* **2015**, 1–11.
[39] M. P. Williamson, *Progress in Nuclear Magnetic Resonance Spectroscopy* **2013**, *73*, 1–16.
[40] T. A. Khrustaleva, *Advances in Bioinformatics* **2014**, *2014*, 1–14.